

Pulsed laser deposited Cr₂O₃ nanostructured thin film on graphene as anode material for lithium-ion batteries

S. Khamlich^{a,b,*}, Z.Y. Nuru^{a,b}, A. Bello^c, M. Fabiane^c, J. K. Dangbegnon^c, N. Manyala^c, M. Maaza^{a,b}

^a UNESCO-UNISA Africa Chair in Nanosciences-Nanotechnology, College of Graduate Studies, University of South Africa, Muckleneuk Ridge, PO Box 392, Pretoria, South Africa

^b Nanosciences African Network (NANOAFNET), iThemba LABS-National Research Foundation, 1 Old Faure Road, Somerset West 7129, PO Box 722, Somerset West, Western Cape Province, South Africa

^c Department of Physics, SARChI Chair in Carbon Technology and Materials, Institute of Applied Materials, University of Pretoria, Pretoria, South Africa

Abstract

Pulsed laser deposition technique was used to deposit Cr₂O₃ nanostructured thin film on a chemical vapour deposited few-layer graphene (FLG) on nickel (Ni) substrate for application as anode material for lithium-ion batteries. The experimental results show that graphene can effectively enhance the electrochemical property of Cr₂O₃. For Cr₂O₃ thin film deposited on Ni (Cr₂O₃/Ni), a discharge capacity of 747.8 mA h g⁻¹ can be delivered during the first lithiation process. After growing Cr₂O₃ thin film on FLG/Ni, the initial discharge capacity of Cr₂O₃/FLG/Ni was improved to 1234.5 mA h g⁻¹. The reversible lithium storage capacity of the as-grown material is 692.2 mA h g⁻¹ after 100 cycles, which is much higher than that of Cr₂O₃/Ni (111.3 mA h g⁻¹). This study reveals the differences between the two material systems and emphasizes the role of the graphene layers in improving the electrochemical stability of the Cr₂O₃ nanostructured thin film.

Keywords: Chromium (III) oxide, Anode, Graphene, lithium-ion batteries,

Corresponding authors: S. Khamlich,

Emails: skhamlich@gmail.com

1. Introduction

Rechargeable lithium ion batteries are integral to the portable, entertainment, computing, and telecommunication equipment required by today's information-rich, mobile society [1]. They are currently one of the most popular types of battery for portable electronic devices due to their light weight, high energy density, high power, smooth discharge, and being environment friendly [2]. However, the fact that their performance, in terms of energy and power density requires continuous improvement has encouraged ever-greater scientific efforts toward the search for new materials that could replace the current state-of-the-art materials [3]. A large number of transition metal oxides, such as Fe_2O_3 [4], Nb_2O_5 [5], Ta_2O_5 [6], ZnO [7], MnO [8], NiO [9], Co_3O_4 [10], Cu_2O [11], have been investigated as promising anode materials for lithium-ion batteries [12]. In 2000, Poizot et al. [13] reported that nanosized transition metal oxides react reversibly with lithium at room temperature. This reaction mechanism existed in many transition metal-oxide systems, such as CoO , Co_3O_4 , FeO , and NiO . Later, this mechanism was further confirmed by Obrovac et al. [14] during their investigation of nanosized $\alpha\text{-LiFeO}_2$, $\beta\text{-Li}_5\text{FeO}_4$ and CoO powder electrodes by in-situ XRD and Mössbauer measurements. Thin film is a very unique system wherein to study these materials based on the conversion reaction. There are three distinct advantages for these thin-film electrodes. First, they are free from additives and binders, so they offer an unmixed condition within which to investigate a material's intrinsic characteristics. Second, the films are easy to fabricate. Third, they can be deposited on a current collector assuring extensive contact between the active particles and the substrate. The contact is much better than that of powder materials. Li and coworkers [15] fabricated thin-film electrodes of pseudo binary mischmetal-Fe-O libraries by combinatorial sputtering methods. They proved that doping transition-metal oxides with rare earth metals lowers the working potential of the former, but results in lower reversible capacities. Co_3O_4 thin films synthesized by different technologies exhibited different reaction mechanisms [16-19]. Thus, Co_3O_4 thin films prepared by PLD demonstrated reversible conversion between Co_3O_4 and $\text{Co/Li}_2\text{O}$ [16,17], while Co_3O_4 thin films prepared by electrolytic deposition were converted into CoO after the initial cycle instead of Co_3O_4 [18,19].

Compared with other transition metal oxides, Cr_2O_3 has become one of the promising lithium storage candidates due to its high theoretical capacity of 1058 mA h g^{-1} and relative low electromotive force value of 1.08 V [20]. However, its application in practical lithium-ion

batteries is still hindered by the low electronic conductivity and severe volume change during repeated discharge/charge processes, which result in serious disintegration of electrode and rapid deterioration of cyclic performance [21]. Several strategies have been developed to alleviate the volume change and increase the conductivity of the electrode, including the preparation of nanoscale materials (e.g., Cr_2O_3 nanoparticles) [22], hollow or mesoporous materials (e.g., mesoporous Cr_2O_3) [23,24], and carbon-based composites (e.g., carbon-coated Cr_2O_3) [25,26]. Recently, a novel two-dimensional carbon matrix (i.e., graphene) has attracted tremendous attention and is preferable to replace other carbon materials (e.g., graphite) for supporting metal and metal oxides due to its excellent properties such as high electrical conductivities, unique mechanical properties and large specific surface areas [27,28]. The properties of active materials can be improved considerably through the synergistic effects of graphene and active materials [29,30]. For instance, graphene-based metal oxides usually exhibit excellent electrochemical performances as electrode materials for LIBs because the graphene substrate may enhance the electronic conductivity of the overall electrode and buffer the strain from the volume variation of metal oxides during lithiation and delithiation processes [31–35].

In this paper, we describe a new and different approach for the fabrication of an anode material system that comprises pulsed laser-deposited (PLD) Cr_2O_3 grown on few layer graphene (FLG) by chemical vapor deposition (CVD). The graphene layers serve as an underlying conducting layer for Cr_2O_3 . The substrate was nickel, a material that has generated recent interest as a current collector [36, 37]. CVD graphene offers the advantage of large area coverage over exfoliated graphite [38]. Specifically, our investigation offers the advantages of large area FLG coverage on a planar substrate, well-characterized graphene and PLD nanostructured Cr_2O_3 thin film, and a comparison of the performance of PLD Cr_2O_3 as an anode material with and without underlying graphene layers. To the best of our knowledge there are no previous reports of the combination of PLD Cr_2O_3 with FLG as anode material. The growth and characterization of this $\text{Cr}_2\text{O}_3/\text{FLG}/\text{Ni}$ material system for application as an anode in lithium ion batteries is described.

2. Experiments and Methods

2.1. CVD Growth of few-layer graphene on nickel substrate

Poly-Ni substrates were chosen in our work because of their availability in large sizes and low cost. Poly-Ni substrate in sizes of 10 cm 10 cm (Ni foil, 0.5 mm thick, 99.98% metals basis) were purchased from Sigma-Aldrich. The Poly-Ni substrate was cut into 15.5 mm diameter disks (to fit into the coin cell for the electrochemical measurements) and placed in a quartz tube of outer diameter 5 cm and inner diameter 4.5 cm. The precursor gases were CH₄, H₂ and Ar. The nickel substrate was annealed at 800 °C in the presence of Ar and H₂ for 20 min, before the introduction of the CH₄ gas at 1000 °C. The flow rates of the gases CH₄, H₂ and Ar were 10, 10 and 300 sccm, respectively. After 15 min of deposition, the sample was rapidly cooled by pushing the quartz tube to a lower temperature region.

2.2. Growth of Cr₂O₃ nanostructured thin film on Ni and FLG/Ni

The PLD setup used for the synthesis of Cr₂O₃ nanostructured thin films is the SURFACE Laser Workstation which consists of a Lambda Physik LPX-305icc excimer laser (wavelength=248 nm, 20 ns pulse duration; repetition rate from 1 to 10Hz) coupled to a high vacuum deposition chamber that houses the substrate holder and target manipulator. The laser beam is guided into the chamber through a beam line consisting of two mirrors and a converging lens with a focal distance of 45 cm. The focused laser beam enters the chamber through a quartz window and is incident on the target at an angle of 45°. The laser repetition rate was fixed at 10Hz and the laser spot size on the target was estimated at about 10 mm². A cylindrical pellet “ $\phi = 15$ mm and about 2mm thick” with a composition of Cr₂O₃ Was used as target. The target was prepared from stoichiometric amount of simple oxide Cr₂O₃ powder (99.9%) obtained from Sigma-Aldrich. It was set to rotate and toggle continuously during the ablation process, in order to ensure uniform erosion and reduce target drilling by the laser. The Cr₂O₃ films were deposited on Ni and FLG/Ni discs (15.5 mm diameter and 0.5 mm thickness) placed on a rotating heatable substrate holder at a distance of 50 mm from the target. Before deposition, the chamber is evacuated by a turbo-molecular pump down to a residual pressure of 10⁻⁵ Pa after which the sample is heated to a temperature of 950 °C, as

measured by thermocouple placed on the back of the substrate. Deposition pressure is then fixed to 1.2 Pa, by flowing oxygen gas (purity 99.999%) in the chamber using electronic mass flow controllers. The deposition of Cr₂O₃ nanostructured thin film was performed at laser energy of 200 mJ, in order to reduce to a minimum, the generation of droplets and microparticles in the ablation plume that may end up embedded in the growing layer.

2.3. Material characterization

The structural characterization of the FLG/Ni, and Cr₂O₃/FLG/Ni were investigated by X-ray diffraction (XRD) using a Bruker D8 Advance X-ray diffractometer equipped with Cu K α radiation ($\lambda = 1.5406 \text{ \AA}$), employing a scanning rate of 0.2° s^{-1} and 2θ ranges from 20° to 80° . The Raman spectra were recorded using a WITEC-Alpha 300R Plus confocal Raman spectrometer (WITEC GmbH, Ulm, Germany). The excitation source was a 532 nm laser (2.33 eV, 1 mW power) through a numerical aperture of 0.9 and with 100x magnification. Morphological characterization was performed on a high-resolution Zeiss Ultra Plus 55 field emission gun scanning electron microscope (FE-SEM) operated at 2.0 kV.

For comparison purpose, different electrochemical characterisations were performed for FLG/Ni, Cr₂O₃/Ni and Cr₂O₃/FLG/Ni electrodes during the Li⁺ insertion and extraction in a half cells configuration. All half cells are assembled as CR2032-type coin cells in an argon-filled glove box with the deposited thin films as test electrodes, pure Li foil as a counter electrode, and porous polypropylene (PP) film (Celgrad 2400) as a separator (Fig. 1). The non-aqueous electrolyte used in the cells is 1 M LiPF₆ dissolved in ethylene carbonate (EC) and dimethyl carbonate (DMC) (1:1 weight ratio). Cyclic voltammetry (CV) tests were performed between 0.0 and 3.0 V with a scan rate of 0.2 mV s^{-1} , and the electrochemical impedance spectroscopy (EIS) was carried out in the frequency range from 10 mHz to 100 kHz on an Autolab PGSTAT Workstation 302 (ECO-CHEMIE, Metrohm Autolab BV, Utrecht, the Netherlands) driven by the GPES software. The galvanostatic charge–discharge performance was measured with a LAND test system at room temperature, and the voltage range was from 0.0 to 3.0 V (versus Li/Li⁺), at a current density of 50 mA g^{-1} in a constant temperature chamber (25°C).



Figure 1: A coin cell fabrication process with Ni-grown FLG and FLG/Ni-grown Cr_2O_3

3. Results and discussions

3.1. Structural analysis

Figure 2 shows the XRD patterns of Ni substrate, FLG/Ni and $\text{Cr}_2\text{O}_3/\text{FLG}/\text{Ni}$ respectively. The XRD pattern of the deposited FLG on Ni shows a broad peak at $2\theta = 25.15^\circ$, which is the reflection (002) of graphene. The fairly broad reflection (002) suggests that the graphene sheets stack into few layers and they are very poorly ordered along the stacking direction [39]. Furthermore, The XRD pattern of $\text{Cr}_2\text{O}_3/\text{FLG}/\text{Ni}$ shows that the diffraction peaks of Cr_2O_3 thin film appeared in the 2θ range $30^\circ\text{--}74^\circ$ (Fig. 2). The identification of all Bragg diffraction peaks confirms the crystallographic phase of the Cr_2O_3 nanostructured thin layer and is ascribed to pure rhombohedral structure (JCPDS No. 74-0326) with lattice constants a and c of about $\sim 4.96070 \text{ \AA}$ and $\sim 13.59900 \text{ \AA}$ respectively and space group $R3c$ [40]. The relatively higher and sharper diffraction peaks observed are directly linked to the good crystallinity of the Cr_2O_3 deposited on the FLG/Ni substrate. The strong diffraction peaks at the 2θ values 44.38° , 52.08° and 76.65° are associated with the Ni substrate.

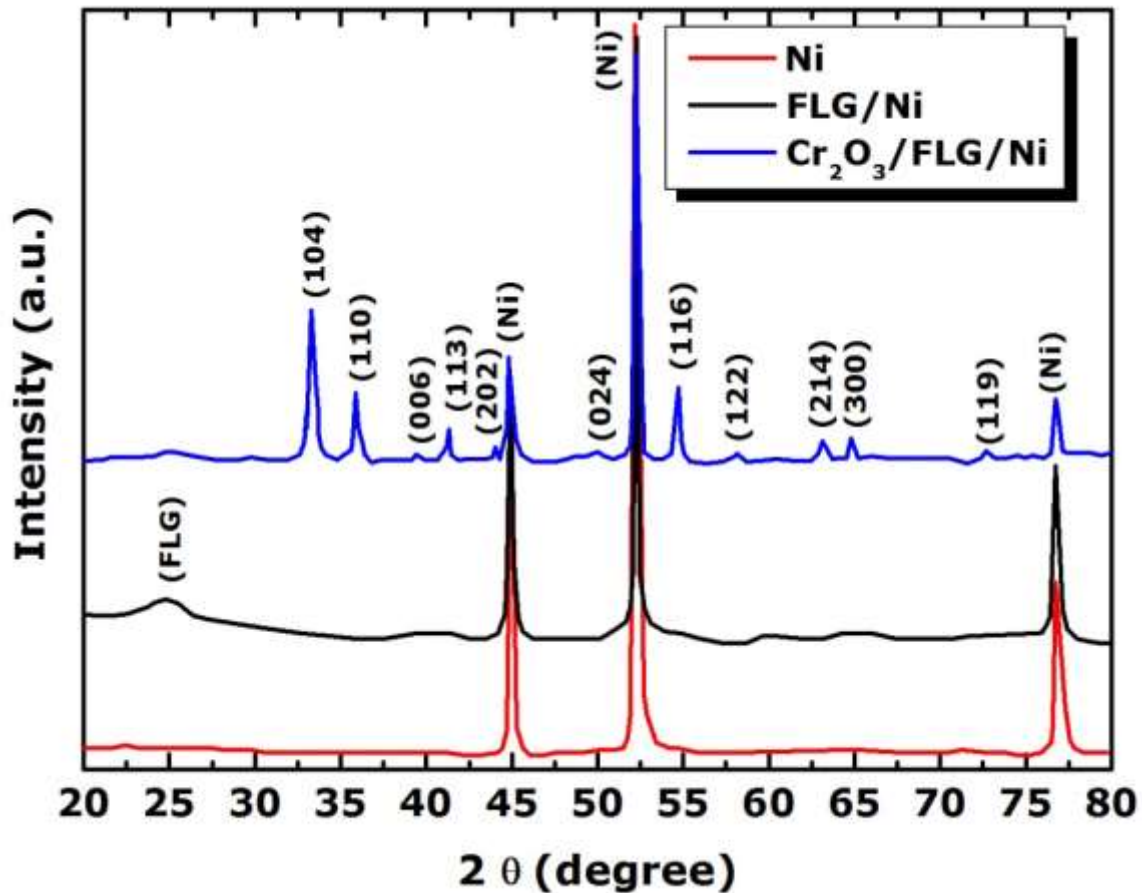


Figure 2: X-ray diffraction patterns of Ni substrate, FLG/Ni and Cr₂O₃/FLG/Ni electrodes.

Figure 3 shows the Raman spectra of the FLG/Ni and Cr₂O₃/FLG/Ni respectively. The Raman spectrum of FLG/Ni shows two prominent peaks at ~ 1591 and 2726 cm^{-1} , corresponding to the characteristic G and 2D bands of graphene [41]. The D band (usually at $\approx 1350\text{ cm}^{-1}$), which is attributed to the disordered graphitic carbon and its intensity, provides information about the density of defects in the as-grown graphene. The fact that the intensity of this band was increased after the deposition of Cr₂O₃ thin film signifies that the PLD deposited Cr₂O₃ induced defects in the structure of graphene. The intensity ratio $I_{2D}/I_G < 1$ indicates that the as-grown graphene is mainly few layered (i.e. it has fewer than five layers) [42]. This is clearly distinguishable from the 2D signal as shown in the inset in Fig. 3 [43]. Moreover, the Raman spectrum of Cr₂O₃/FLG/Ni shows four peaks of Cr₂O₃ at 309 , 352 , 548 and 628 cm^{-1} , which agree very well with what are found in the literature [40]. In this work, we found that all peaks of the PLD deposited Cr₂O₃ nanostructured thin film showed only

three E_g and one A_{1g} modes of chromium (III) oxide (see Fig. 3). The observation of only four modes in the sample is due to the polycrystallinity of Cr_2O_3 thin film [40].

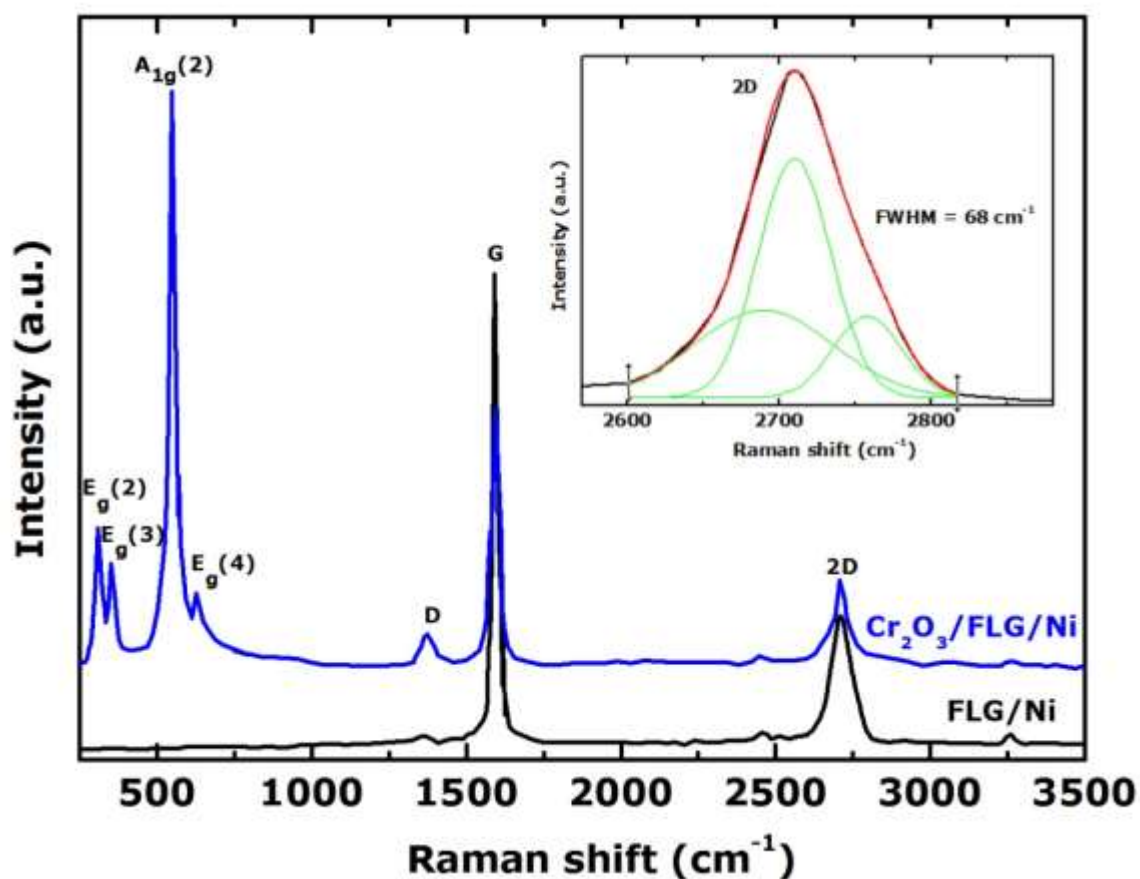


Figure 3: Raman spectra of FLG/Ni and Cr_2O_3 /FLG/Ni electrodes.

3.2. Morphological analysis

The SEM micrographs in Figure 4 clearly show the typical morphologies of the Ni substrate, FLG/Ni and the PLD deposited Cr_2O_3 nanostructured thin film on FLG/Ni. It can be seen from Fig. 4(a) that the Ni substrate has a very smooth surface. Fig. 4(b) displays a representative sample of the as-grown graphene on Ni substrate. After the CVD process, graphene layers with different wrinkles were coated on the smooth surface of the Ni. In the Cr_2O_3 /FLG/Ni sample, nanostructured Cr_2O_3 is densely deposited onto FLG/Ni surface (Fig.

4(c)). The film appears dense and devoid of any droplets or macro-particulates. Statistical analysis of the microimage indicates that the average grain size L_c is about 180 nm. Fig. 4(d)

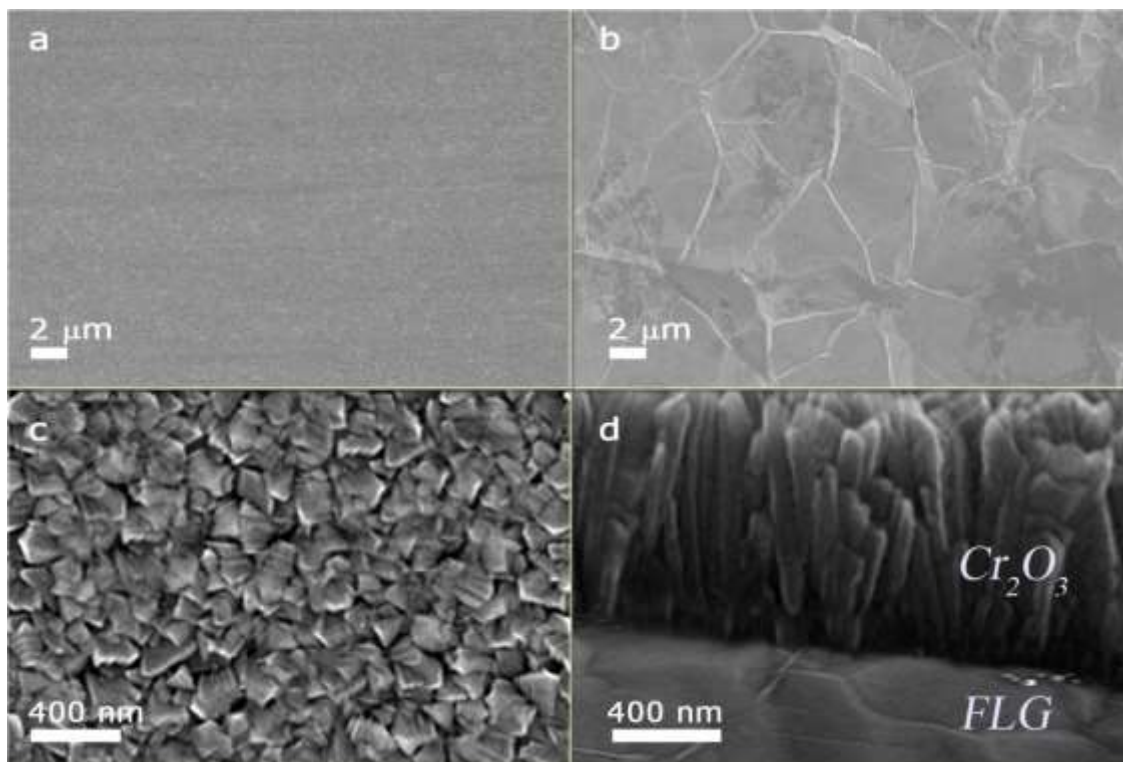


Figure 4: FE-SEM micrographs of (a) Ni substrate; (b) FLG deposited on Ni; (c) shows a high-magnification view of Cr₂O₃ nanostructured thin film; (d) Cross-section view of Cr₂O₃/FLG anode.

shows a cross-section view of the SEM image of Cr₂O₃/FLG/Ni sample. The 745 nm thick Cr₂O₃ film and many columnar nanostructures perpendicular to the FLG/Ni surface are observed. Moreover, the nanostructured nature of the deposited film could shorten the diffusion length of lithium ions in Cr₂O₃ and improve charge transport during alloying and dealloying of Cr₂O₃ with lithium [44].

3.3. Electrochemical analyses

Figure 5 compares the cyclic voltammetry (CV) curves of Ni substrate, FLG/Ni, Cr₂O₃/Ni and Cr₂O₃/FLG/Ni measured in a potential window of 0– 0.3 V at scan rate of 0.2 mV·s⁻¹. Ni substrate itself showed very poor CV measurements and the FLG/Ni electrode measured

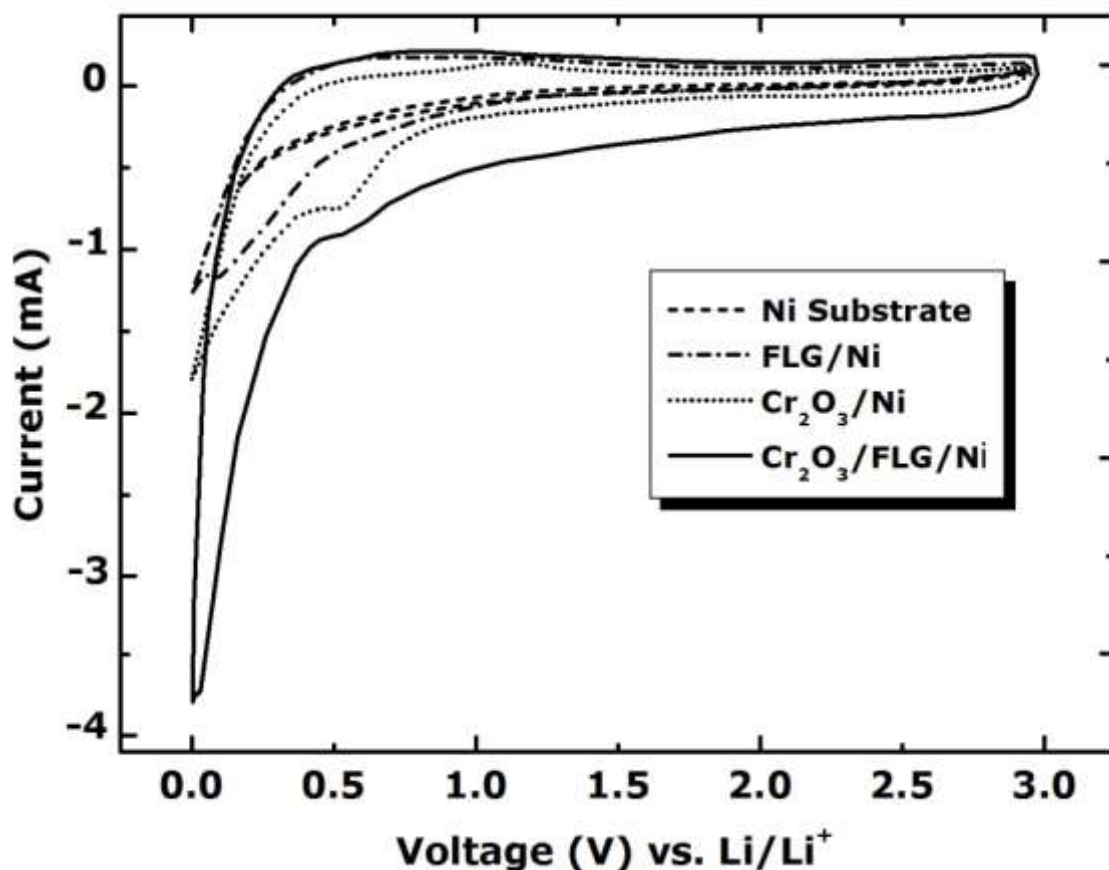


Figure 5: CV curves of Ni substrate, FLG/Ni, Cr₂O₃/Ni and Cr₂O₃/FLG/Ni measured in a potential window of 0–0.3 V at scan rate of 0.2 mV s⁻¹.

under the same conditions exhibited low-intensity current peaks around 0.1 V due to the interaction of Li with graphene [35], and also to the quasi-super hydrophobicity which is attributed to poor surface wetting and thus the reduced accessibility and utilisation of the available surface area [41]. The CV curve of Cr₂O₃/Ni in Fig. 5 shows a reduction peak at 0.47 V during the cathodic scan and two oxidation peaks appears around 2.12 V and 1.07 V during the anodic scan, representing the lithiation/delithiation reaction in the active material. Compared with the curve of the Cr₂O₃/Ni, that of the Cr₂O₃/FLG/Ni composite showed that the peak corresponding to the reduction of Cr₂O₃ shifted to high potential of 0.64 V, which can be attributed to the presence of graphene [45].

Figure 6a and b shows the CV of Cr₂O₃ nanostructured thin film and Cr₂O₃/FLG electrodes deposited on Ni substrate in the voltage range of 0–3.0 V at a scan rate of 0.2 mV·s⁻¹ during the first five charge-discharge cycles. As shown in Figure 6 (a,b), the performance of anodic and cathodic in the first cycle is quite different from the following cycles possibly owing to

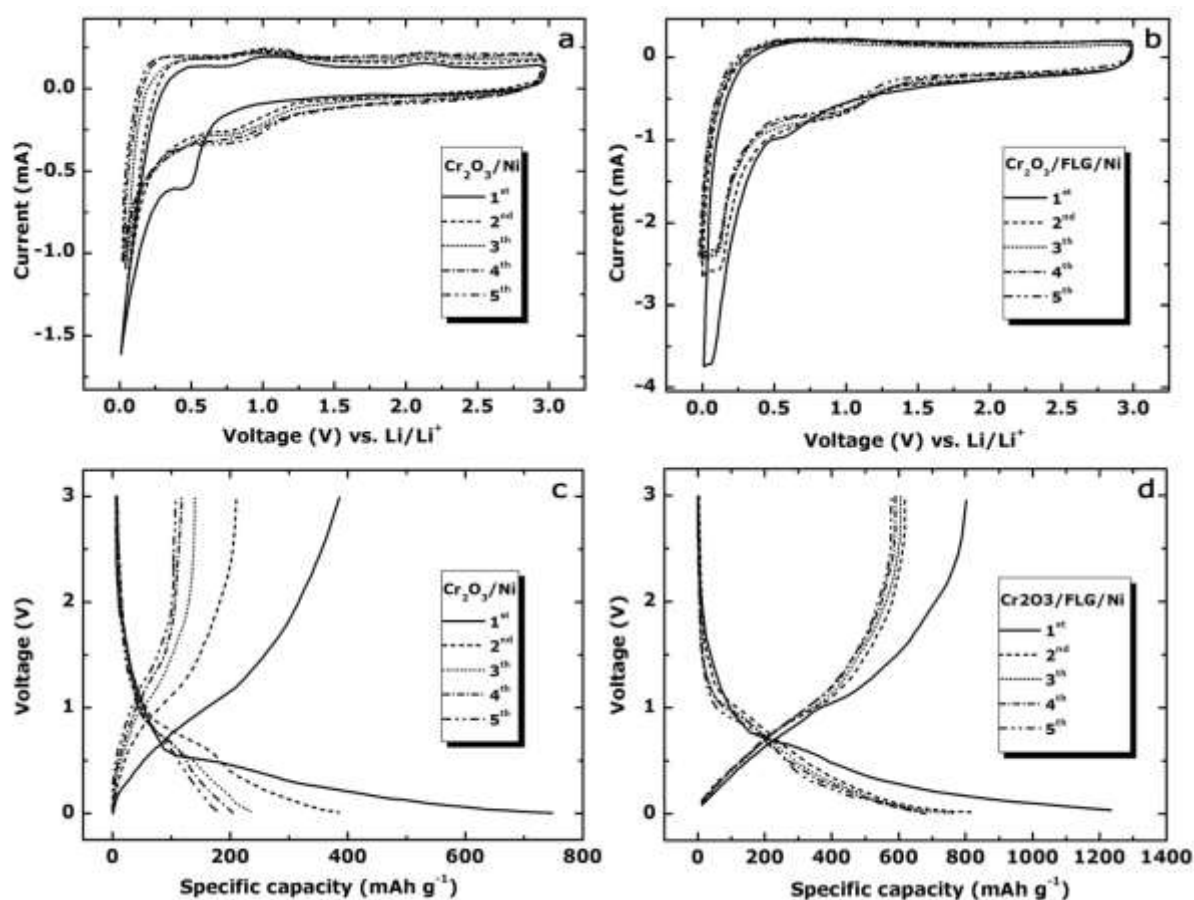


Figure 6: (a,b) CV curves of $\text{Cr}_2\text{O}_3/\text{Ni}$ and $\text{Cr}_2\text{O}_3/\text{FLG}/\text{Ni}$ electrodes in the voltage range of 0–3.0 V at a scan rate of $0.2 \text{ mV}\cdot\text{s}^{-1}$ during the first five charge-discharge cycles; (c,d) discharge/charge profiles of $\text{Cr}_2\text{O}_3/\text{Ni}$ and $\text{Cr}_2\text{O}_3/\text{FLG}/\text{Ni}$ in the initial 5 cycles at room temperature and constant current density of 50 mA g^{-1} .

the formation of a solid electrolyte interface (SEI) on the surface of the active materials. Moreover, the first cathodic sweep of figure 6a exhibited a distinct reduction peak at $\sim 0.47 \text{ V}$, which was related to the first electrochemical process of Cr_2O_3 , including its reduction and the formation of the SEI layer. In the first anodic sweep, two peaks observed at around 1.07 V and 2.12 V indicated the partial decomposition of the SEI layer and the reoxidation of Cr [24,26]. Moreover, from the 2nd cycle to the 5th cycle the redox peaks are almost unchanged and shifted to a higher potential at around 0.88 V , and the electrochemical reactions were reversible. Figure 6b shows the CV profiles of $\text{Cr}_2\text{O}_3/\text{FLG}/\text{Ni}$ from the 1st to the 5th cycle. The peak corresponding to the reduction of Cr_2O_3 appeared at around 0.64 V in the first cathodic sweep, and shifted to a potential at around 0.96 V in subsequent cycles. Another reduction

peak was observed near 0.06 V, which was assigned to the insertion of Li^+ into graphene [35].

The discharge/charge profiles of $\text{Cr}_2\text{O}_3/\text{Ni}$ and $\text{Cr}_2\text{O}_3/\text{FLG}/\text{Ni}$ in the initial 5 cycles at room temperature and constant current density of 50 mA g^{-1} are shown in Figure 6c and d respectively. During the discharge process, both samples showed only one plateau at around 0.54 V corresponding to the transformation of Cr_2O_3 and Li^+ to Cr and Li_2O , which is in good agreement with the Li-storage mechanism of other Cr_2O_3 -based anodes [23], and then a sloping voltage profile from 0.54 V to the lower cut-off voltage of 0.0 V during the first discharge process, and a sloping voltage plateau between 0.7 and 1.12 V during the reverse charge process, which are consistent with the redox peaks in the cyclic voltammetry profiles. The first charge and discharge capacities were around 385.6 and 747.8 mA h g^{-1} for $\text{Cr}_2\text{O}_3/\text{Ni}$ which was higher than what was reported in the literature [23], 801.6 and 1234.5 mA h g^{-1} for $\text{Cr}_2\text{O}_3/\text{FLG}/\text{Ni}$, these results shows that graphene improves the charge/discharge performance of this anode material both, in the first and the followed charge /discharge profiles. This improved electrochemical performance can be mainly attributed to the high electrical conductivity of graphene and the nanostructured nature of Cr_2O_3 thin film on the graphene. The nanostructured nature of the active material was clearly contributing to the electrochemical performance in H. Liu *et al.*, study [24] due to the high surface area to volume ratio of nanomaterials which provides a tremendous driving force for electrolyte diffusion. They reported that the as-prepared nanoporous Cr_2O_3 materials exhibit enhanced performance for lithium ion batteries compared to the bulk Cr_2O_3 .

Figure 7 shows the cycle performances of FLG/Ni , $\text{Cr}_2\text{O}_3/\text{Ni}$ and $\text{Cr}_2\text{O}_3/\text{FLG}/\text{Ni}$ at current density of 50 mA g^{-1} . The capacity of FLG/Ni after 100 cycles was 324 mA h g^{-1} , Much smaller than that of $\text{Cr}_2\text{O}_3/\text{FLG}/\text{Ni}$ ($\sim 692.2 \text{ mA h g}^{-1}$). On the other hand, the capacity of $\text{Cr}_2\text{O}_3/\text{Ni}$ decreased rapidly to $\sim 123.9 \text{ mA h g}^{-1}$ after only 12 cycles. On the contrary, $\text{Cr}_2\text{O}_3/\text{FLG}/\text{Ni}$ showed good cycling stability and high stable reversible capacities, e.g., $\sim 692.2 \text{ mA h g}^{-1}$ after 100 cycles, which was still higher than the capacity of carbon-based anodes ($\sim 290 \text{ mA h g}^{-1}$) [46]. As expected, FLG material effectively buffered the strain from the volume variation of Cr_2O_3 , leading to the improvement of cycle performance of Cr_2O_3 [35]. Furthermore, Zhou et al. [47] reported that C–O–Cr bridge between Cr_2O_3 and graphene might also contribute to the improvement of the electrochemical performance. The improved electrochemical performance of $\text{Cr}_2\text{O}_3/\text{FLG}/\text{Ni}$ can be assigned to the synergistic effects of

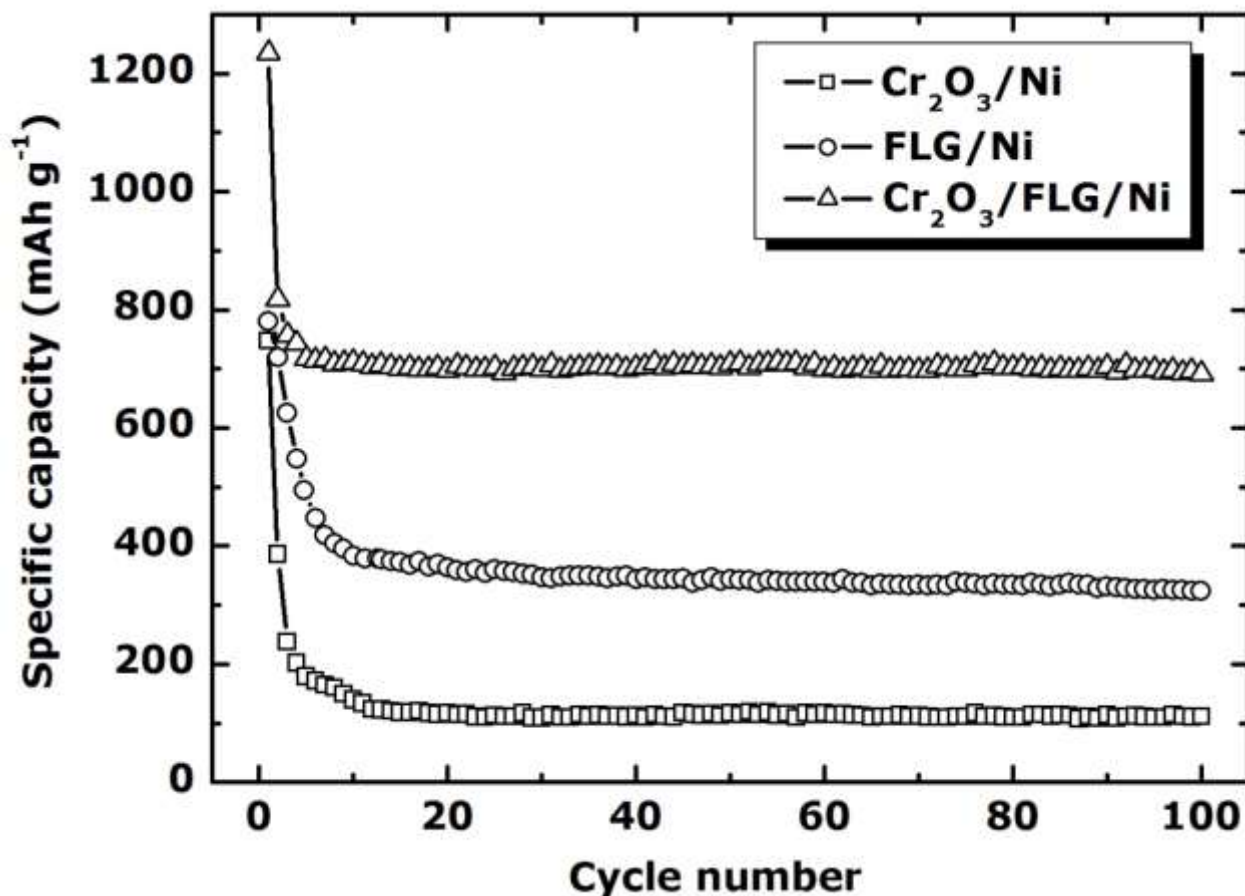


Figure 7: The cycle performances of FLG/Ni, Cr₂O₃/Ni and Cr₂O₃/FLG/Ni at current density of 50 mA g⁻¹.

graphene and Cr₂O₃. Namely, pulsed laser deposition technique used to deposit Cr₂O₃ thin film on FLG provides good crystallinity, uniformity and adhesion which gives rise to a high electrical conductivity of the overall electrode and accommodate the volume expansion of Cr₂O₃ nanostructured thin film during the cycling [48,49]. The impedance spectra of the Cr₂O₃/Ni and Cr₂O₃/FLG/Ni electrodes at the end of the charge in the 100th cycle are shown in Fig. 8. They are similar to each other in shape, with a semicircle in the intermediate frequency region and a straight line in the low frequency region. This semicircle in the medium frequency region can be assigned to the charge-transfer impedance on Cr₂O₃ electrode/electrolyte interface. Obviously, the impedance in the Cr₂O₃/FLG/Ni electrode is smaller than in the Cr₂O₃/Ni electrode, meaning the FLG/Ni supported electrode is more advantageous than the Ni supported one to reduce the charge-transfer impedance. Therefore, the Cr₂O₃/FLG/Ni electrode shows a more excellent electrochemical performance. Cycled at higher rates, Cr₂O₃/FLG/Ni electrode still reveals outstanding electrochemical performance

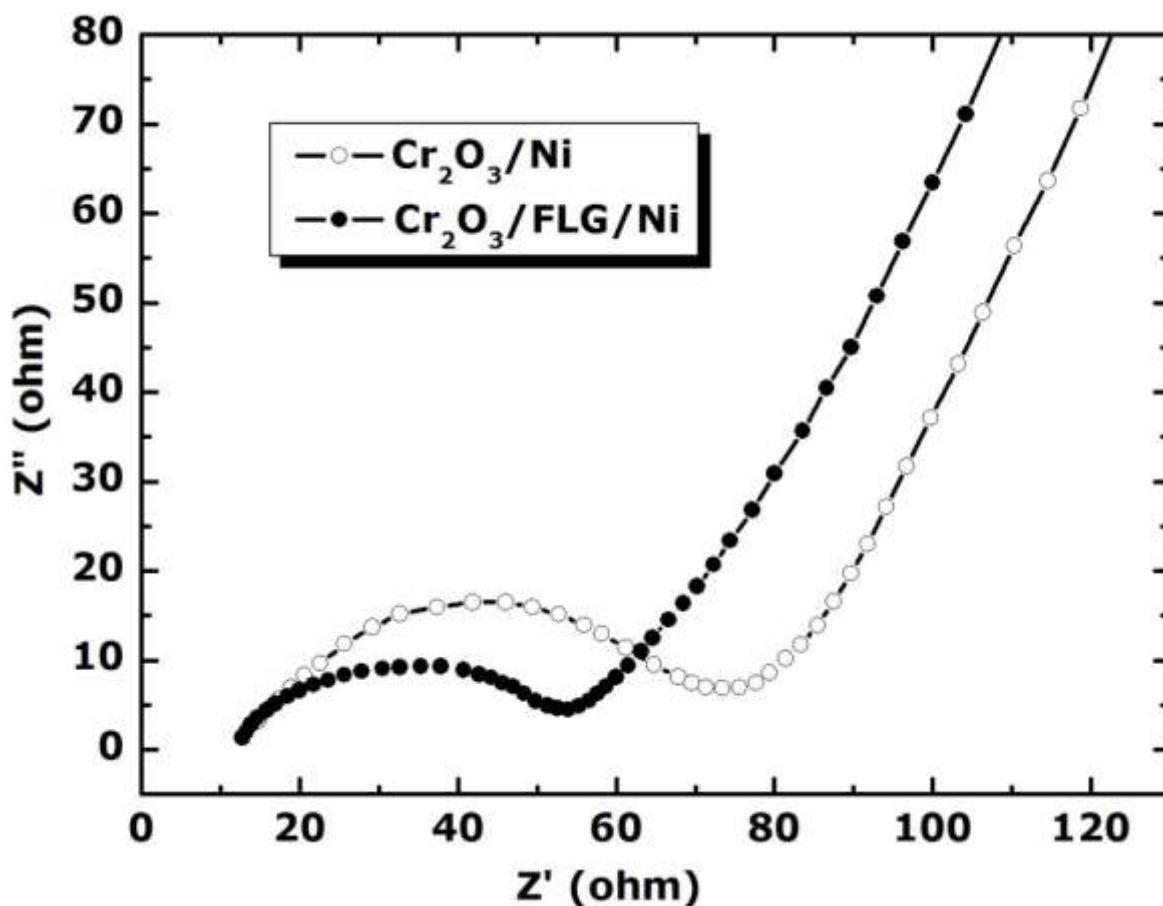


Figure 8: The impedance spectra of the Cr₂O₃/Ni and Cr₂O₃/FLG/Ni electrodes at the end of the charge in the 100th cycle

as shown in Fig. 9. It can deliver the reversible capacities of 589.7, 534.2, 472.3, and 378.8 mA h g⁻¹ at 100, 200, 300 and 400 mA g⁻¹, respectively. Additionally, a capacity of 543.6 mA h g⁻¹ was retained after 50 cycles when the current density recovered to 100 mA g⁻¹, also implying its good cycling stability. This result means that graphene plays an important role in the improvement of the cycling performance of Cr₂O₃/FLG/Ni anode material. In order to confirm the structural stability of the deposited materials, Raman analysis for FLG/Ni and Cr₂O₃/FLG/Ni were performed after 50 cycles as shown in Fig. 10 and Fig. 11, respectively. The relative D-, G- and 2D-peak heights change noticeably for the cycled FLG/Ni anode. The D-band intensity increases substantially, the G-band broadens and increased slightly and the 2D-band decreased. These results revealed some degree of degradation in the FLG after the cycling. Moreover, the Raman spectral of Cr₂O₃/FLG/Ni anode (Fig. 11) clearly displays a decrease in E_g and A_{1g} modes of chromium (III) oxide, which might be results of formation of a solid electrolyte interface (SEI) on the surface of Cr₂O₃ nanostructured thin film. These

results confirmed that the active material electrode still reveals outstanding structural stability which contributed to its good electrochemical and cycling stability.

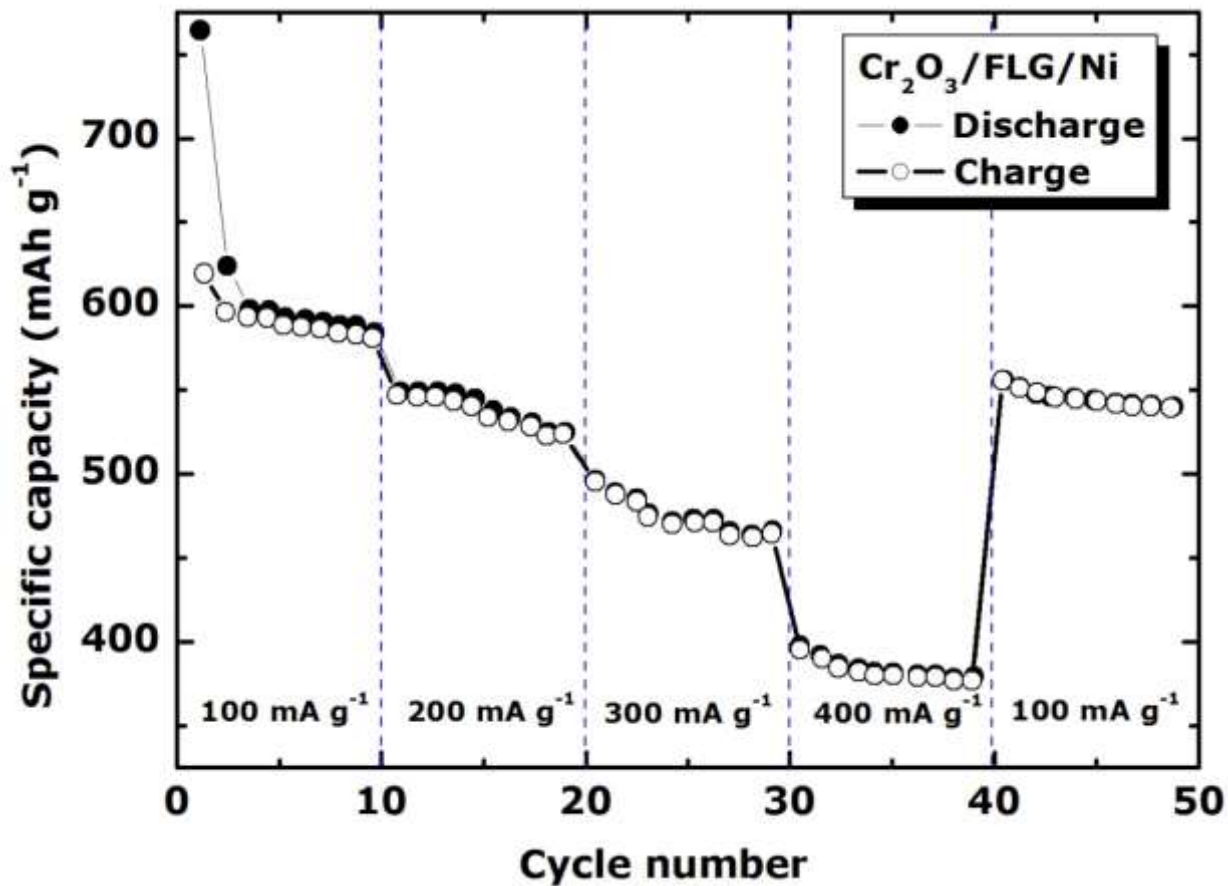


Figure 9: Rate performances of Cr₂O₃/FLG/Ni electrode

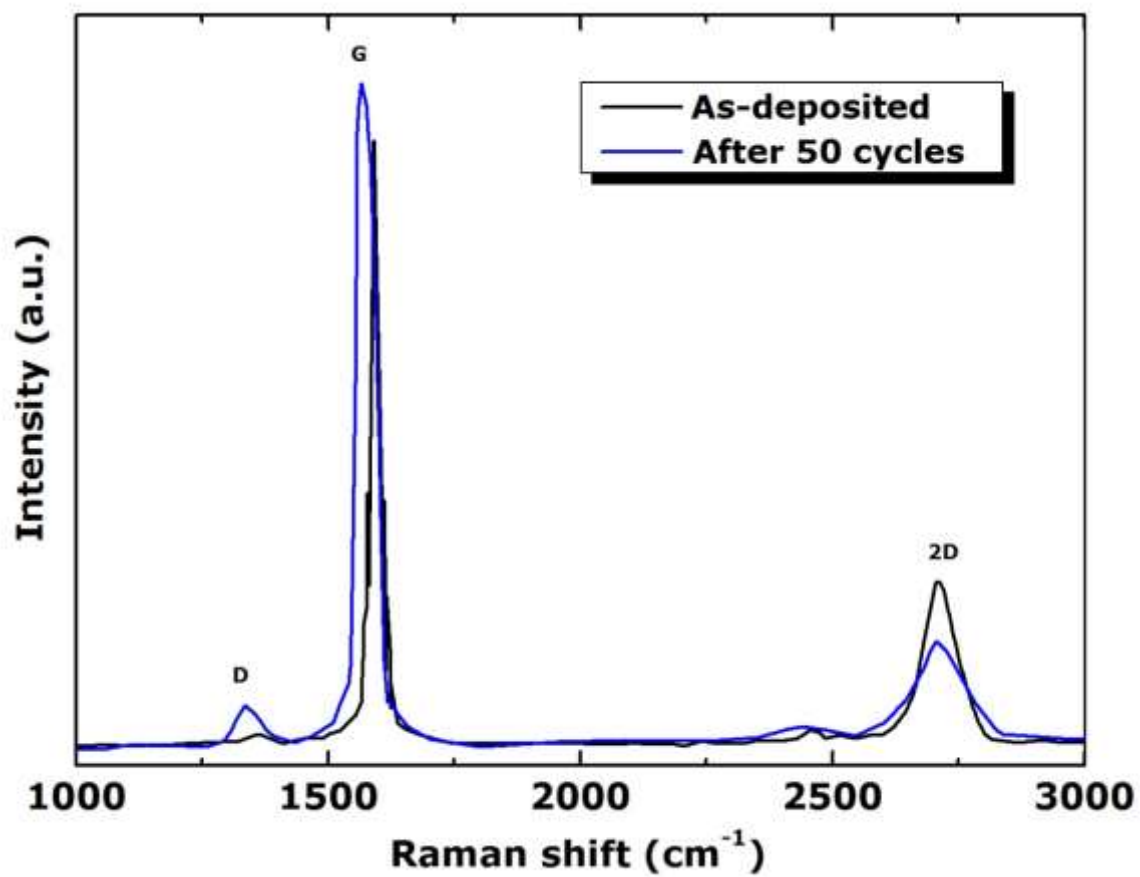


Figure 10: Raman spectra of FLG/Ni as-deposited and after 50 cycles.

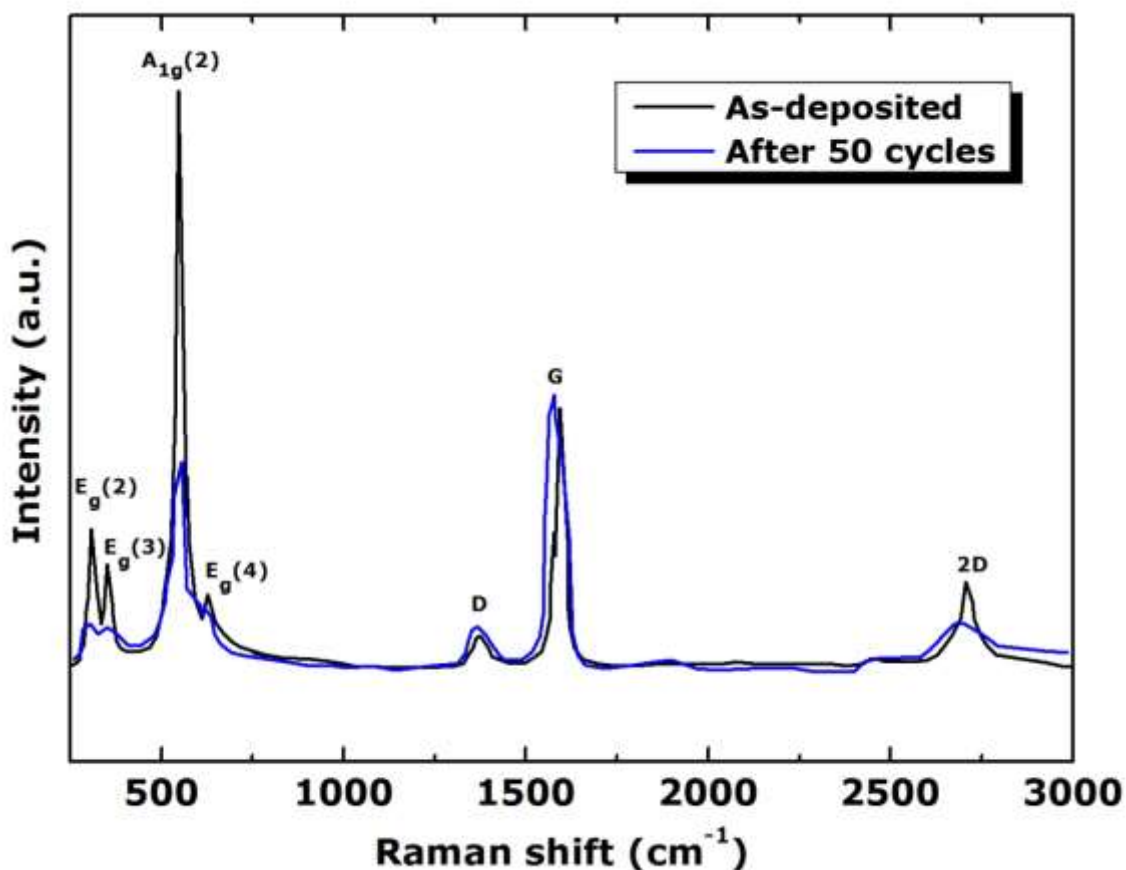


Figure 11: Raman spectra of Cr₂O₃/FLG/Ni as-deposited and after 50 cycles.

4. Conclusion

Through this paper, we have shown the advantages of chemical vapour deposited few layer graphene (FLG) in improving the electrochemical performance of Cr₂O₃ nanostructured thin film. The improved electrochemical performance of Cr₂O₃ can be assigned to the synergistic effects of graphene and Cr₂O₃. Namely, pulsed laser deposition technique used to deposit Cr₂O₃ on FLG provides good crystallinity, uniformity and adhesion which gives rise to a high electrical conductivity of the overall electrode and accommodate the volume expansion of Cr₂O₃ nanostructured thin film during the cycling. The high reversible capacity, small irreversible capacity loss and good stable cycle of Cr₂O₃/FLG/Ni electrode make it one of the promise anode materials for future lithium-ion batteries.

Acknowledgements

This work was sponsored within the framework of the UNESCO UNISA Africa Chair in Nanosciences & Nanotechnology and the Nanosciences African Network (NANOAFNET) by the National Research Foundation of South Africa, the African Laser Centre (ALC), the University of South Africa (UNISA) in collaboration with the Vice-Chancellor of the University of Pretoria, the National Research Foundation (NRF) of South Africa, iThemba LABS and the Abdus Salam ICTP-Trieste, Italy.

Reference

- [1] R. Teki, M.K. Datta, R. Krishnan, T.C. Parker, T.M. Lu, P.N. Kumta, N. Koratkar, *Small* 5 (2009) 2236-2242.
- [2] N. Zhou, M. Z. Xue, Z. W. Fu, *J. Power Sources* 234 (2013) 310-332.
- [3] J. Cabana, Z. Stoeva, J.J. Titman, D.H. Gregory, M.R. Palacín, *Chem. Mater.* 20 (2008) 1676-1678.
- [4] B.T. Hang, I. Watanabe, T. Doi, S. Okada, J.-I. Yamaki, *J. Power Sources* 161 (2006) 1281-1287.
- [5] M.D. Wei, K. Wei, M. Ichihara, H.S. Zhou, *Electrochem. Commun.* 10 (2008) 980-983.
- [6] Z.W. Fu, F. Huang, Y.Q. Chu, Y. Zhang, Q.Z. Qin, *J. Electrochem. Soc.* 150 (2003) A776-A782.
- [7] Z.W. Fu, F. Huang, Y. Zhang, Y. Chu, Q.Z. Qin, *J. Electrochem. Soc.* 150 (2003) A714-A720.
- [8] X.Q. Yu, Y. He, J.P. Sun, K. Tang, H. Li, L.Q. Chen, X.J. Huang, *Electrochem. Commun.* 11 (2009) 791-794.
- [9] B. Varghese, M.V. Reddy, Y.W. Zhu, C.S. Lit, T.C. Hoong, G.V. Subba Rao, B.V.R. Chowdari, A.T. Shen Wee, C.T. Lim, C.-H. Sow, *Chem. Mater.* 20 (2008) 3360-3367.

- [10] Z.W. Fu, Y. Wang, Y. Zhang, Q.Z. Qin, *Solid State Ionics* 170 (2004) 105-109.
- [11] J.Y. Xiang, J.P. Tu, Y.F. Yuan, X.H. Huang, Y. Zhou, L. Su YZ, *Electrochem. Commun.* 11 (2009) 262-265.
- [12] W.J. Li, Z.W. Fu, *Appl. Surf. Sci.* 256 (2010) 2447–2452.
- [13] P. Poizot, S. Laruelle, S. Grugeon, L. Dupont, J.M. Tarascon, *Nature* 407 (2000) 496-499.
- [14] M.N. Obrovac, R.A. Dunlap, R.J. Sanderson, J.R. Dahn, *J. Electrochem. Soc.* 148 (2001) A576-A588.
- [15] J. Li, H.M. Dahn, R.J. Sanderson, A.D.W. Todd, J.R. Dahn, *J. Electrochem. Soc.* 155 (2008) A975-A981.
- [16] V. Pralong, J.B. Leriche, B. Beaudoin, E. Naudin, M. Morcrette, J.M. Tarascon, *Solid State Ionics* 166 (2004) 295-305.
- [17] Y. Wang, Z.W. Fu, Q.Z. Qin, *Thin Solid Films* 441 (2003) 19-24.
- [18] H.C. Liu, S.K. Yen, *J. Power Sources* 166 (2007) 478-484.
- [19] S.L. Chou, J.Z. Wang, H.K. Liu, S.X. Dou, *J. Power Sources* 182 (2008) 359-364.
- [20] B.K. Guo, M.F. Chi, X.G. Sun, S. Dai, *J. Power Sources* 205 (2012) 495–499.
- [21] J. Hu, H. Li, X.J. Huang, *Electrochem. Solid-State Lett.* 8 (2005) A66–A69.
- [22] J. Hu, H. Li, X.J. Huang, L.Q. Chen, *Solid State Ionics* 177 (2006) 2791-2799.
- [23] L. Dupont, S. Laruelle, S. Grugeon, C. Dickinson, W.Z. Zhou, J.M. Tarascon, *J. Power Sources* 175 (2008) 502–509.
- [24] H. Liu, X.W. Du, X.R. Xing, G.X. Wang, S.Z. Qiao, *Chem. Commun.* 48 (2012) 865–867.
- [25] L.Y. Jiang, S. Xin, X.L. Wu, H. Li, Y.G. Guo, L.J. Wan, *J. Mater. Chem.* 20 (2010) 7565–7569.
- [26] B.K. Guo, M.F. Chi, X.G. Sun, S. Dai, *J. Power Sources* 205 (2012) 495–499.

- [27] A.K. Geim, K.S. Novoselov, *Nat. Mater* 6 (2007) 183–191.
- [28] K.S. Novoselov, A.K. Geim, S.V. Morozov, D. Jiang, M.I. Katsnelson, I.V. Grigorieva, S. V. Dubonos, A.A. Firsov, *Nature* 438 (2005) 197–200.
- [29] N. Li, Z.F. Geng, M.H. Cao, L. Ren, X.Y. Zhao, B. Liu, Y. Tian, C.W. Hu, *Carbon* 54 (2013) 124–132.
- [30] L.N. Gao, W.B. Yue, S.S. Tao, L.Z. Fan, *Langmuir* 29 (2013) 957–964.
- [31] D.Y. Zhai, B.H. Li, H.D. Du, G.Y. Gao, L. Gan, Y.B. He, Q.H. Yang, F.Y. Kang, *Carbon* 50 (2012) 5034–5043.
- [32] T. Hu, X. Sun, H.T. Sun, M.P. Yu, F.Y. Lu, C.S. Liu, J. Lian, *Carbon* 51 (2013) 322–326.
- [33] W.B. Yue, S. Yang, Y. Ren, X.J. Yang, *Electrochim. Acta* 92 (2013) 412–420.
- [34] W.B. Yue, S. Yang, Y.L. Liu, X.J. Yang, *Mater. Res. Bull.* 48 (2013) 1575–1580.
- [35] W. Yue, S. Tao, J. Fu, Z. Gao, Y. Ren, *Carbon* 25 (2013) 97–104.
- [36] X. Liu, D. Wang, S. Shi, *Electrochim. Acta* 87 (2013) 865–871.
- [37] Q. Sa and Y. Wang, *J. Power Sources* 208 (2012) 46–51.
- [38] A. Reina, X. Jia, J. Ho, D. Nezich, H. Son, V. Bulovic, M. S. Dresselhaus, J. Kong, *Nano Letters* 9 (2009) 30–35.
- [39] Y. Wang, S. Gao, X. Zang, J. Li, J. Ma, *Analytica. Chimica. Acta* 716 (2012) 112–118.
- [40] S. Khamlich, E. Manikandan, B. D. Ngom, J. Sithole, O. Nemraoui, I. Zorkani, R. McCrindle, N. Cingo, M. Maaza, *J. Phys. Chem. Solids* 72 (2011) 714–718.
- [41] S. Khamlich, A. Bello, M. Fabiane, B. D. Ngom, N. Manyala, *J Solid State Electrochem.* 17 (2013) 2879–2886.
- [42] D. Wei, J.I. Mitchell, C. Tansarawiput, W. Nam, M. Qi, P.D. Ye, X. Xu, *Carbon* 53 (2013) 374–379.

- [43] A. Reina, X.T. Jia, J. Ho, D. Nezich, H. Son, V. Bulovic, M.S. Dresselhaus, J. Kong, *Nano Lett.* 9 (2009) 30-35.
- [44] M. Park, X. Zhang, M. Chung, G. B. Less, A. M. Sastry, *J. of Power Sources* 195 (2010) 7904-7929.
- [45] X.Y. Xue, C.H. Ma, C.X. Cui, L.L. Xing High, *Solid State Sciences* 13 (2011) 1526-1530.
- [46] M. Wakihara, *Mater. Sci. Eng. R33* (2001) 109-134.
- [47] G.M. Zhou, D.W. Wang, L.C. Yin, N. Li, F. Li, H.M. Cheng, *ACS Nano* 6 (2012) 3214-3223.
- [48] C.F. Zhang, X. Peng, Z.P. Guo, C.B. Cai, Z.X. Chen, D. Wexler, S. Li, H. K. Liu, *Carbon* 50 (2012) 1897-1903.
- [49] Y.Z. Su, S. Li, D.Q. Wu, F. Zhang, H.W. Liang, P.F. Gao, C. Cheng, X. L. Feng, *ACS Nano* 6 (2012) 8349-8356.